

Influence of focal point properties on energy transfer and plasma evolution during laser ignition process with a passively q-switched laser

MARK BÄRWINKEL,* SEBASTIAN LORENZ, ROBERT STÄGLICH, AND DIETER BRÜGGEMANN

University of Bayreuth, Chair of Engineering Thermodynamics and Transport Processes,
Universitätsstraße 30, 95447 Bayreuth, Germany

*lttt@uni-bayreuth.de

Abstract: Miniaturized passively q-switched laser ignition systems are a promising alternative to conventional ignition sources to ensure a reliable ignition under difficult conditions. In this study the influences of focal point properties on energy transfer from laser to plasma as well as plasma formation and propagation are investigated as the first steps of the laser induced ignition process. Maximum fluence and fluence volume are introduced to characterize focal point properties for varying laser pulse energies and focusing configurations. The results show that the transferred laser energy increases with increasing maximum fluence. During laser emission plasma propagates along the beam path of the focused laser beam. Rising maximum fluence results in increased plasma volume, but expansion saturates when fluence volume reaches its maximum.

©2016 Optical Society of America

OCIS codes: (140.0140) Lasers and laser optics; (140.3480) Lasers, diode-pumped; (140.3540) Lasers, Q-switched; (140.3440) Laser-induced breakdown; (350.5400) Plasmas.

References and links

- G. Dearden and T. Shenton, "Laser ignited engines: progress, challenges and prospects," *Opt. Express* **21**(S6 Suppl 6), A1113–A1125 (2013).
- J. Fuchs, A. Leitner, G. Tinschmann, and C. Trapp, "Concept for high-performance direct ignition gas engines," *MTZ worldwide* **74**(5), 18–23 (2013).
- J. Tauer, H. Kofler, and E. Wintner, "Laser-initiated ignition," *Laser Photonics Rev.* **4**(1), 99–122 (2010).
- E. Albin, H. Nawroth, S. Göke, Y. D'Angelo, and C. O. Paschereit, "Experimental investigation of burning velocities of ultra-wet methane-air-steam mixtures," *Fuel Process. Technol.* **107**, 27–35 (2013).
- E. Mastorakos, "Ignition of turbulent non-premixed flames," *Prog. Energ. Combust.* **35**(1), 57–97 (2009).
- S. Lorenz, M. Bärwinkel, R. Stäglich, W. Mühlbauer, and D. Brüggemann, "Pulse train ignition with passively Q-switched laser spark plugs," *Int. J. Engine Res.* **17**(1), 139–150 (2016).
- M. S. Bak, S. Im, and M. A. Cappelli, "Successive laser-induced breakdowns in atmospheric pressure air and premixed ethane-air mixtures," *Combust. Flame* **161**(7), 1744–1751 (2014).
- N. Kawahara, J. L. Beduneau, T. Nakayama, E. Tomita, and Y. Ikeda, "Spatially, temporally, and spectrally resolved measurement of laser-induced plasma in air," *Appl. Phys. B* **86**(4), 605–614 (2007).
- C. V. Bindhu, S. S. Harilal, M. S. Tillack, F. Najmabadi, and A. C. Gaeris, "Energy absorption and propagation in laser-created sparks," *Appl. Spectrosc.* **58**(6), 719–726 (2004).
- J.-L. Beduneau and Y. Ikeda, "Spatial characterization of laser-induced sparks in air," *J. Quant. Spectrosc. Radiat. Transf.* **84**(2), 123–139 (2004).
- M. Weinrotter, H. Kopecek, E. Wintner, M. Lackner, and F. Winter, "Application of laser ignition to hydrogen-air mixtures at high pressures," *Int. J. Hydrogen Energy* **30**(3), 319–326 (2005).
- H. Kopecek, H. Maier, G. Reider, F. Winter, and E. Wintner, "Laser ignition of methane-air mixtures at high pressures," *Exp. Therm. Fluid Sci.* **27**(4), 499–503 (2003).
- D. K. Srivastava, E. Wintner, and A. K. Agarwal, "Effect of laser pulse energy on the laser ignition of compressed natural gas fueled engine," *Opt. Eng.* **53**(5), 056120 (2014).
- D. K. Srivastava, E. Wintner, and A. K. Agarwal, "Effect of focal size on the laser ignition of compressed natural gas-air mixture," *Opt. Lasers Eng.* **58**, 67–79 (2014).
- J. D. Mullett, R. Dodd, C. J. Williams, G. Triantos, G. Dearden, A. T. Shenton, K. G. Watkins, S. D. Carroll, A. D. Scarisbrick, and S. Keen, "The influence of beam energy, mode and focal length on the control of laser ignition in an internal combustion engine," *J. Phys. D Appl. Phys.* **40**(15), 4730–4739 (2007).
- H. Kofler, J. Tauer, G. Tartar, K. Iskra, J. Klausner, G. Herdin, and E. Wintner, "An innovative solid-state laser for engine ignition," *Laser Phys. Lett.* **4**(4), 322–327 (2007).

17. N. Pavel, M. Tsunekane, and T. Taira, "Composite, all-ceramics, high-peak power Nd:YAG/Cr⁴⁺:YAG monolithic micro-laser with multiple-beam output for engine ignition," *Opt. Express* **19**(10), 9378–9384 (2011).
18. M. Tsunekane, T. Inohara, A. Ando, N. Kido, K. Kanehara, and T. Taira, "High peak power, passively Q-switched microlaser for ignition of engines," *IEEE J. Quantum Electron.* **46**(2), 277–284 (2010).
19. G. Kroupa, F. Georg, and W. Ernst, "Novel miniaturized high-energy Nd-YAG laser for spark ignition in internal combustion engines," *Opt. Eng.* **48**(1), 014202 (2009).
20. J. Schwarz, K. Stoppel, K.-H. Nübel, and J. Engelhardt, "Pumping concepts for laser spark plugs - requirements, options, solutions," presented at OPIC 2014 – 2nd Laser Ignition Conference (2014).
21. S. Lorenz, M. Bärwinkel, P. Heinz, S. Lehmann, W. Mühlbauer, and D. Brüggemann, "Characterization of energy transfer for passively Q-switched laser ignition," *Opt. Express* **23**(3), 2647–2659 (2015).
22. D. Y. Tang, S. P. Ng, L. J. Qin, and X. L. Meng, "Deterministic chaos in a diode-pumped Nd:YAG laser passively Q switched by a Cr⁴⁺:YAG crystal," *Opt. Lett.* **28**(5), 325–327 (2003).
23. N. Pavel, T. Dascalu, G. Salamu, M. Dinca, N. Boicea, and A. Birtas, "Ignition of an automobile engine by high-peak power Nd:YAG/Cr⁴⁺:YAG laser-spark devices," *Opt. Express* **23**(26), 33028–33037 (2015).
24. T. Alger, D. Mehta, C. Chadwell, and C. Roberts, "Laser ignition in a pre-mixed engine: The effect of focal volume and energy density on stability and the lean operating limit," *SAE Technical Paper*, 2005–01–3752 (2005).
25. J. X. Ma, D. R. Alexander, and D. E. Poulain, "Laser spark ignition and combustion characteristics of methane-air mixtures," *Combust. Flame* **112**(4), 492–506 (1998).
26. M. Börner, C. Manfletti, and M. Oschwald, "Laser re-ignition of a cryogenic multi-injector rocket engine," in 6th European Conference for Aeronautics and Space Sciences (2015).
27. S. H. Lee, H. Do, and J. J. Yoh, "Simultaneous optical ignition and spectroscopy of a two-phase spray flame," *Combust. Flame* **165**, 334–345 (2016).
28. ISO 11146–1:2005(E), "Lasers and laser-related equipment - Test methods for laser beam widths, divergence angles and beam propagation ratios - Part 1: Stigmatic and simple astigmatic beams," (2005).
29. J. Ostrinsky and H. Ridderbusch, and Robert Bosch GmbH, "Laser Ignition System," WO/2014/122281 (07.02.2014).
30. E. Hecht, *Optics* (Addison-Wesley, 2002).
31. W. M. Steen and J. Mazumder, *Laser Material Processing* (Springer London, 2010).
32. S. Brieschenk, H. Kleine, and S. O'Byrne, "On the measurement of laser-induced plasma breakdown thresholds," *J. Appl. Phys.* **114**(9), 093101 (2013).
33. L. J. Radziemski and D. A. Cremers, *Laser-Induced Plasmas and Applications* (M. Dekker, 1989).
34. T. X. Phuoc and F. P. White, "Laser-induced spark ignition of CH₄/air mixtures," *Combust. Flame* **119**(3), 203–216 (1999).
35. Y. P. Raizer, "Breakdown and heating of gases under the influence of a laser beam," *Sov. Phys. Usp.* **8**(5), 650–673 (1966).
36. E. Yablonovitch, "Self-phase modulation and short-pulse generation from laser-breakdown plasmas," *Phys. Rev. A* **10**(5), 1888–1895 (1974).
37. Y. P. Raizer, "Heating of a gas by a powerful light pulse," *J. Exp. Theor. Phys.* **21**, 1009–1017 (1965).
38. T. X. Phuoc, "Laser spark ignition: experimental determination of laser-induced breakdown thresholds of combustion gases," *Opt. Commun.* **175**(4–6), 419–423 (2000).
39. S. A. Ramsden and P. Savic, "A radiative detonation model for the development of a laser-induced spark in air," *Nature* **203**(4951), 1217–1219 (1964).
40. T. X. Phuoc, "An experimental and numerical study of laser-induced spark in air," *Opt. Lasers Eng.* **43**(2), 113–129 (2005).
41. N. Glumac, G. Elliott, and M. Boguszko, "Temporal and spatial evolution of a laser spark in air," *AIAA J.* **43**(9), 1984–1994 (2005).
42. Y.-L. Chen, J. Lewis, and C. Parigger, "Spatial and temporal profiles of pulsed laser-induced air plasma emissions," *J. Quant. Spectrosc. Radiat. Transf.* **67**(2), 91–103 (2000).
43. J. Tang, D. Zuo, T. Wu, and Z. Cheng, "Spatio-temporal evolution of laser-induced air plasma in the stage of laser pulse action," *Opt. Commun.* **289**, 114–118 (2013).
44. S. Brieschenk, S. O'Byrne, and H. Kleine, "Visualization of jet development in laser-induced plasmas," *Opt. Lett.* **38**(5), 664–666 (2013).
45. C. G. Morgan, "Laser-induced breakdown of gases," *Rep. Prog. Phys.* **38**(5), 621–665 (1975).
46. L. R. Evans and C. G. Morgan, "Lens aberration effects in optical-frequency breakdown of gases," *Phys. Rev. Lett.* **22**(21), 1099–1102 (1969).

1. Introduction

Current engine development strategies are dominated by increasing efficiency and by reduction of pollutant emissions because of regulatory tightening [1]. Stratified charge engines and large gas engines use lean combustion to achieve these objectives [2,3], resulting in longer combustion durations and lower power density of the engine. To avoid efficiency losses, the grade of turbulence and the boost pressure can be increased [4]. These measures increase the demands for the ignition system [5]. Laser induced ignition is a promising option to meet demands of a future ignition source. Miniaturized passively q-switched laser (PQL)

spark plugs additionally have the potential to meet the requirements regarding cost-effectiveness and robustness [6].

Such a laser ignition system is built up from a pulsed laser and one or more lenses for converging the laser beam. Therefore, not only laser parameters like pulse energy and beam quality affect the ignition and combustion process, but also focusing parameters like effective focal length. Several researchers already investigated these effects:

Bak et al. [7] measured the laser energy absorbed by the plasma for different laser energies between 7.5 mJ and 60 mJ and focal lengths of converging lens of 50 mm, 100 mm and 150 mm. Absorption grows with higher incident laser energies. A shorter focal length leads to a slightly higher absorption at incident laser energies less than 30 mJ as well as a slightly lower absorption at incident laser energy exceeding 30 mJ.

Kawahara et al. [8] showed the effect of increased laser pulse energy on the plasma growth time and the plasma volume in air, which both are proportional to the incident pulse energy. Increased plasma volume at higher pulse energies is also demonstrated by Bindhu et al. [9]. Fluctuations of plasma size and location of the edges of the plasma were observed by Beduneau et al. [10] and were correlated with the optical configuration for different focal lengths of 50 mm, 100 mm and 300 mm. Fluctuations are greater for a long focal length, but the plasma size is simultaneously increased. A large plasma size is considered to be beneficial for ignition efficiency. Weinrotter et al. [11] demonstrated that an enlarged plasma size, which is caused by higher focal length, decrease the total combustion time of a hydrogen-air mixture, however, the minimum pulse energy for ignition (MPE) increased.

In the study of Kopecek et al. [12], MPE of methane-air mixtures was determined for different focal lengths. A shorter focal length results in a decreased MPE, but, after a certain value, a further decrease of the focal length does not cause a further reduction of MPE. Srivastava et al. [13] investigated the effect of laser pulse energy on laser ignition of a compressed natural gas in a combustion chamber and an engine. The combustion duration was shortened by using higher pulse energies. The ignition delay decreased and the maximum cylinder pressure and the rate of heat release increased with rising laser pulse energy. In another study [14], they pointed out that the focal length has a significant influence on the MPE. It is shown that longer focal lengths are accompanied by increased MPE. The combustion duration is shorter for a focal length of 150 mm compared to 100 mm and 200 mm for all investigated air ratios. Engine tests have shown a higher maximum cylinder pressure and rate of heat release for focal length of 30 mm compared to 50 mm. Mullett et al. [15] have applied laser ignition to one cylinder of a four-cylinder gasoline engine using a q-switched Nd:YAG laser operating in three different beam modes associated with the cavity aperture diameter. Best results have been achieved by utilizing short focal length and a high laser cavity aperture diameter. Advantages consist in a decreased coefficient of variance of the indicated mean effective pressure and the variance in the peak cylinder pressure position.

It is evident that laser pulse energy and focusing parameters have a significant influence on the laser induced ignition and the combustion process. In all discussed studies actively q-switched lasers (AQL) for laboratory applications and converging lenses with large focal length up to 300 mm are used for laser ignition. AQL do not offer an acceptable price, robustness or design size for a marketable ignition system, but as mentioned before, PQL have the potential to meet these requirements. In recent years, several PQL and PQL ignition systems have been introduced [16–20]. The application of PQL for ignition brings up some challenges to the measurement techniques. On the one hand, PQL have a complex temporal pulse profile. Lorenz et al. [21] have characterized the energy transfer of PQL pulses to plasma temporally and spatially highly resolved. They have demonstrated the influence of the temporal pulse shape on the energy transfer process. On the other hand, a characteristic of a passively q-switched laser pulse is the temporal fluctuation to its optical pump pulse in the range of a few microseconds [18,22]. In engine application, such a jitter is negligible, but it is highly relevant by temporal detection on sub-nanosecond timescales of energy transfer and plasma evolution.

Recently, Pavel et al. [23] have successfully demonstrated the application of a PQL ignition system for ignition of an automobile engine. The influence of pump optics line is discussed in detail, but the effect of focusing configuration on the ignition and combustion process is not examined. In this study, the emphasis is on the investigation of the influence of the focusing configuration on the energy transfer and plasma evolution. Laser pulse energies up to 9 mJ and an effective focal length in the range of 6 mm to 15 mm are used. The applied PQL is first characterized regarding the beam quality factor (M^2) and the beam width for different pulse energies. Maximum fluence and fluence volume are introduced to characterize focal spot properties for varying focusing configurations. In other studies [10,24,25] the focal volume is used to characterize the focal point, but this method only describes the geometry of the focal point and does not consider the pulse energy. Energy transfer measurements are performed and correlated with the above mentioned focal spot properties. Furthermore, a measurement technique is introduced for temporally and spatially highly resolved plasma imaging during energy transfer despite the occurring temporal laser pulse jitter. To the authors knowledge this is the first time plasma evolution can be examined during laser pulse by using a PQL. The determination of the exact breakdown location is important in different engine applications. For example, Börner et al. [26] pointed out, that the tolerance for plasma displacement is only about ± 1 mm for reliable laser ignition of a cryogenic multi-injector rocket engine. In case of direct injection engines, the location of the ignition source is of great importance, due to the inherent engine properties like inhomogeneous equivalence ratio and difficult flow conditions [27]. In the last section, plasma propagation after laser pulse emission is determined quantitatively for different laser pulse energies and focusing configurations.

2. Experimental setup

All investigations are performed with a passively q-switched Nd:YAG/Cr⁴⁺:YAG solid state laser provided by the Robert Bosch GmbH. The Nd:YAG laser is end pumped by a fiber coupled laser diode of 808 nm wavelength and emits nanosecond laser pulses at 1064 nm for the generation of laser sparks. The design of the laser ignition system is shown in Fig. 1. Laser and focusing units are separated. The coupling efficiency of the pump beam into the Nd:YAG crystal can be modified by the position of the optical fiber end and the focusing lens. Hence, the output laser energy is modifiable. The adjustable energy is in the range of 1.5 mJ to 12.0 mJ by this method for the applied laser system. However, it has to be mentioned that the laser pulse properties differs significantly for high laser energies above 9.0 mJ.

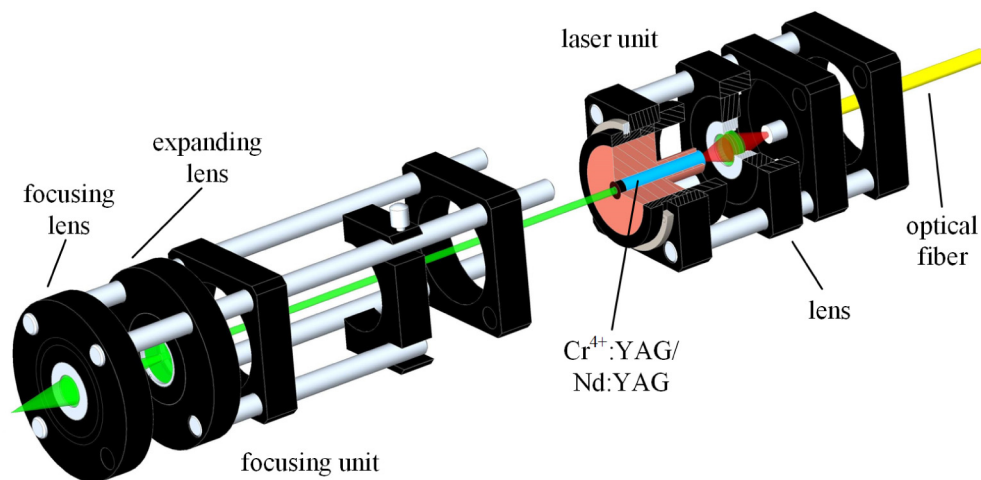


Fig. 1. Design of the passively q-switched laser ignition system

The focusing unit is built up from a plano-concave lens to expand the laser beam and a plano-convex lens for the focusing of laser beam with a focal length of -20 mm and 12 mm, respectively. All lenses are coated with an anti-reflection layer to minimize reflection losses. The distance between the two lenses is also variable. Therefore, laser pulse energy and focusing properties can be varied independently of each other.

Experiments are performed in air and under ambient conditions. Laser crystal is heated up to 40 °C and the pump laser runs repetitively at a frequency of 10 Hz. In the next sections, the experimental setup for energy transfer measurements and plasma imaging are outlined.

2.1 Measurement of energy transfer

The transferred energy from laser beam to plasma is the difference between the overall laser pulse energy and the transmitted laser energy after breakdown. To determine the transferred energy of laser into plasma at different laser pulse energies and focusing parameters, the same experimental setup as applied by Lorenz et al. [21] is used. In Fig. 2, the experimental setup is shown. The transmitted laser beam after breakdown is parallelized and afterwards focused on a fast photodiode (UPD-35-IR2-P, Alphas) linked with a digital storage oscilloscope (DSO, Wavemaster 8Zi-A, LeCroy). Diffusors and a band pass filter for laser wavelength (BP1064) are placed in the detection box in front of the photodiode. For measuring the laser energy without breakdown, the focusing unit is replaced by a concave lens to expand the laser beam.

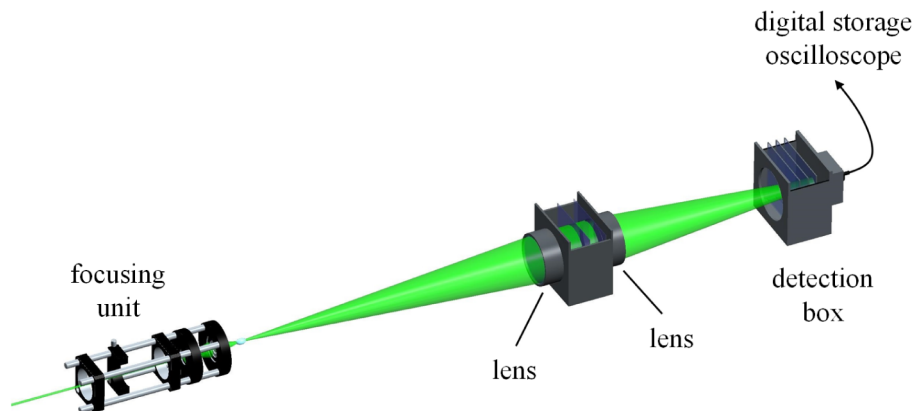


Fig. 2. Experimental setup for energy transfer measurements.

2.2 Plasma imaging

Investigations of plasma evolution are carried out during and after the laser pulse. Figure 3 shows the experimental setup. An occurring plasma shape is focused with a lens system onto an intensified CCD camera (PI-MAX4: 512EM-HBf). As the arising laser emission bleaches the saturable absorber of the passive q-switch, an inevitable temporal jitter of a few microseconds occurs between pump and laser pulses. In engine application, this fluctuation has not to be concerned, but it is a challenge for measuring plasma evolution shortly after the laser pulse with a precision of a tenth of a nanosecond. The laser pulse is transduced into an electric trigger signal via a fast photodiode (SIR5-FC, Thorlabs). Two different measuring techniques were developed to record plasma images at different time scales. The camera is triggered by the laser pulse for plasma imaging after a minimum delay of 32 ns (internal temporal delay of camera and delay due to cables and trigger equipment). To achieve recordings at earlier times, especially during energy transfer, camera and laser are operating in a random mode. Therefore, laser and camera are triggered with a fixed delay to each other. The laser signal of the fast photodiode and the monitor signal of the camera are recorded by a DSO. Thus, laser pulse signal can be matched with the record time of the plasma image and relevant images recorded earlier than 32 ns after laser pulse are filtered.

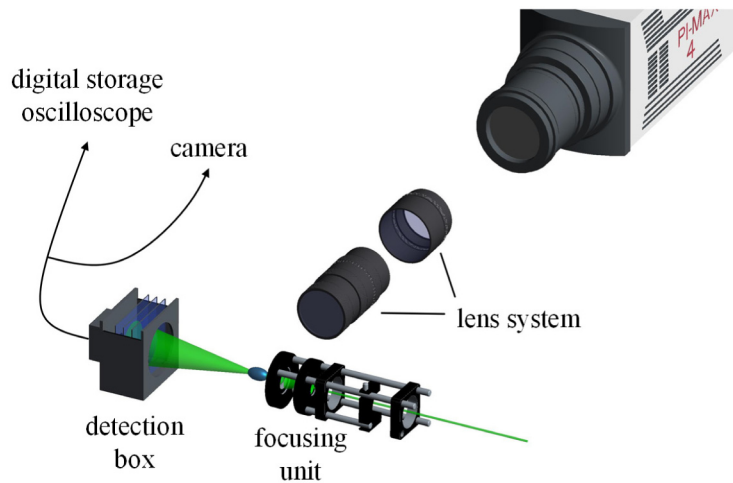


Fig. 3. Experimental setup for plasma imaging

3. Characterization of laser pulses and calculation of focal point properties

In the following chapters achieved results are presented and discussed. In this chapter, laser pulses of different energies are characterized. Based on these results, focal point properties are calculated for varying pulse energies and focusing configurations.

Experiments were performed with laser energies of 3.0 mJ, 4.7 mJ, 6.2 mJ and 9.0 mJ. In Table 1 the properties of the different laser pulses are given. Laser beam width d_{laser} and laser beam quality factor M^2 are measured with a camera based beam propagation analyzer (M²-200s, Ophir Photonics) and interpreted with the 4 Sigma method [28].

A distinction is made between two scenarios: On the one hand, experiments with laser pulses with similar pulse properties are done to demonstrate the influence of pulse energy. On the other hand, the influence of different pulse properties on the investigated issues is demonstrated with an additional example.

In the first scenario laser pulses with an energy of 3.0 mJ, 4.7 mJ and 6.2 mJ are applied. Table 1 shows that laser beam width d_{laser} and beam quality factor M^2 are comparable for these laser pulses. In the second scenario an additional laser pulse with an energy of 9.0 mJ is introduced with significantly higher beam width d_{laser} and beam quality factor M^2 . The difference in the beam quality of the applied laser pulses is also demonstrated in Fig. 4. The 2D-beam intensity profiles of laser pulses up to 6.2 mJ confirm the high beam quality. In contrast to laser pulses with lower energy, the 9.0 mJ laser pulse shows strong bulges in the edge of the beam profile. This indicates a worse beam quality. Furthermore, the fluctuation of laser pulse energy ΔE_{laser} is significantly higher for the 9.0 mJ laser pulse. To emphasize the special case of different pulse properties the suffix * is added whenever the 9 mJ* laser pulse is mentioned.

Table 1. Properties of different laser beams.

E_{laser} [mJ]	3.0	4.7	6.2	9.0*
ΔE_{laser} [%]	1.1	1.1	2.9	6.0
d_{laser} [mm]	0.9	1.1	1.1	1.6
M^2 [-]	2.4	2.9	3.3	5.2
FWHM [ns]	2.4	2.6	2.6	2.8

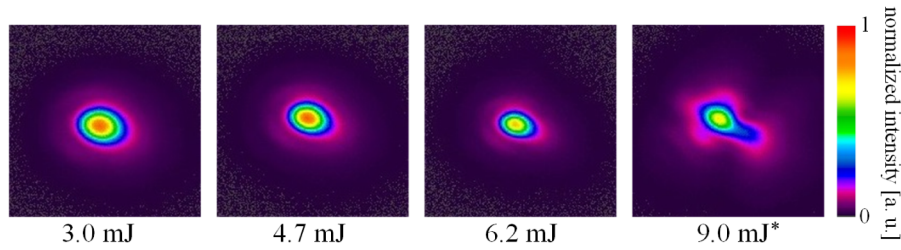


Fig. 4. Cross-sectional beam intensity profiles for different laser energies. (* indicates different pulse properties)

Figure 5 shows the temporal pulse profiles of the different laser pulses recorded by a fast photodiode. It can be seen that maximum power and pulse duration rise with higher pulse energies. Also, the temporal rise in power of the laser beam increases with higher beam energies.

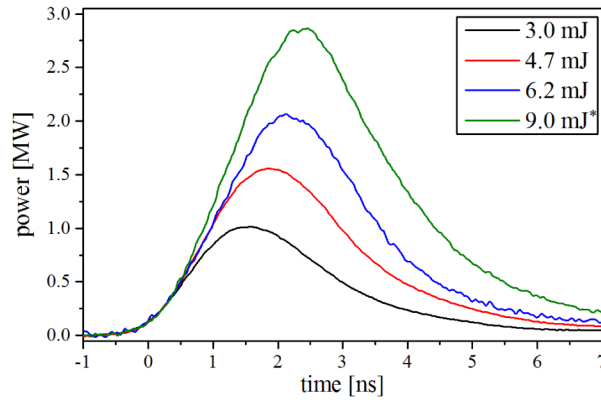


Fig. 5. Temporal laser profiles of laser pulses with different energies. (* indicates different pulse properties)

Focal point characteristics are calculated for different laser energies and distances between expanding and focusing lens. Calculations are done assuming a Gaussian beam profile. Maximum fluence H_{max} and fluence volume V are used to characterize the focal point. The maximum fluence is defined as the maximum energy density in the focal point. A suggestion for calculation of these values is given by Ostrinsky and Ridderbusch [29]:

$$H_{max} = H(z=0) = \frac{2Q}{\pi\omega_0^2} \quad (1)$$

Here, Q is the laser beam energy, ω_0 the minimum beam radius in the focal point (focal radius) and z the distance from the focal point. To calculate the minimum focal radius ω_0 the effective focal length of the focusing unit is required and can be determined by Eq. (2) of [30]

$$\frac{1}{f_{eff}} = \frac{1}{f_1} + \frac{1}{f_2} - \frac{d_{lens}}{f_1 f_2} \quad (2)$$

with f_1 and f_2 being the focal lengths of the concave and converging lens, respectively. The distance between the two lenses is d_{lens} . For calculating the distance between the lenses, the theory for thick lenses is applied. The variation of the lens distance results in effective focal lengths in the range of 6 mm for large lens distances to 15 mm in the case of small lens distances.

Now the minimum focal radius ω_0 can be calculated with [31]:

$$\omega_0 = \frac{2\lambda f_{\text{eff}} M^2}{\pi d_{\text{laser}}} \quad (3)$$

Here, λ is the wavelength of the laser beam, M^2 the beam quality factor and d_{laser} the beam width of the origin laser beam at the surface of the expanding lens. It can be seen that the focal radius is directly proportional to the factor M^2 . Therefore, it is desirable to build lasers with a low beam quality factor (M^2) to obtain a small focal radius.

The second property of the focal region that is influenced by the focusing parameters is the fluence volume V . This is the region in the beam waist in which a characteristic fluence H_{min} is exceeded. The characteristic fluence is different for each gas. In case of air, the characteristic fluence of 15 J/mm² can be chosen [29]. Locations with the same fluence R can be calculated by Eq. (4).

$$R(z) = \omega_0 \sqrt{\left(1 + \frac{z}{z_R}\right)^2 \frac{1}{2} \ln \frac{H_{\text{max}}}{H_{\text{min}} \left(1 + \frac{z}{z_R}\right)^2}} \quad (4)$$

By integration of fluence R one obtains the fluence volume V (Eq. (5)).

$$V = 2\pi \int_0^{z(R=0)} (R(z))^2 dz \quad (5)$$

In Fig. 6(a), the beam waist (red lines), the power density (contour plot) and the fluence volume (white lines) are illustrated for a 4.7 mJ laser pulse and different lens distances. With increasing lens distance the laser beam is more expanded in front of the focusing lens and, therefore, the beam waist is more narrowed. Hence, the power is compressed in a smaller area and the power density increases in the focal region. It should be noted that the power density is normalized to the maximum of each figure.

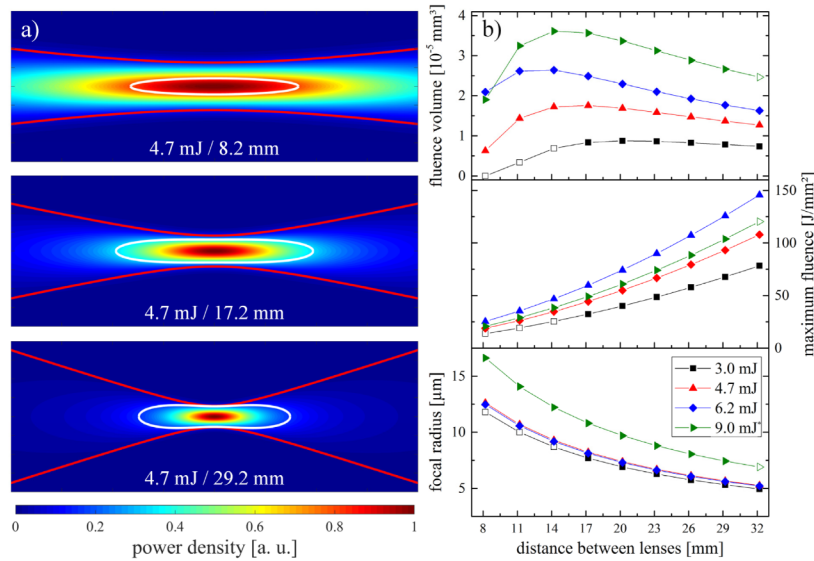


Fig. 6. Calculated focal point properties. (a) beam waist, power density and fluence volume at different lens distances (dimensions: vertical 0.08 mm, horizontal 0.4 mm). (b) focus width, maximum fluence and fluence volume for different lens distances. (* indicates different pulse properties)

Figure 6(b) shows the calculated properties of the focal point. Non-solid symbols represent values without experimental data in the next sections. In case of a 3 mJ laser pulse, no breakdown occurred at lens distances less than 14.2 mm due to insufficient power density. Furthermore, a 9.0 mJ* laser pulse at a lens distance of 32.2 mm is expanded by the concave lens that much that the focusing lens is irradiated inappropriately.

The focal radius decreases with increasing lens distance and is almost identical for laser energies up to 6.2 mJ. The focal radii for a laser pulse energy of 9.0 mJ* are higher than for the lower laser energies. This can be explained by the higher beam quality factor M^2 of the 9.0 mJ* laser pulse resulting in a worse focusability. The maximum fluence increases with increasing lens distance due to a decreasing focal area. The maximum fluences of the 9.0 mJ* laser pulse are below the level of the maximum fluences of 6.2 mJ laser beams because of the higher focal radii due to the worse focusability of the 9.0 mJ* laser pulse.

In the uppermost diagram of Fig. 6(b), the calculated fluence volume is shown for different lens distances. In general, the fluence volume increases for higher laser energies. For a specific laser energy, the fluence volume is on a low level for short lens distances and increases for higher lens distances. Above a certain lens distance, the fluence volume stagnates at a certain value (3 mJ laser energy) or even decreases again slowly (4.7 mJ and 6.2 mJ). By increasing the lens distance, the focal radius is getting smaller and the power density rises, but the region, in which the minimum fluence is exceeded, is reduced simultaneously. Even in the second scenario of different pulse properties (9.0 mJ* laser pulse) the behavior of the fluence volume is similar to laser pulses with better beam quality. Fluence volumes at different lens distances are illustrated in Fig. 6(a) (region within white lines) for a laser energy of 4.7 mJ. It can be seen that the fluence volume is maximum at a lens distance of 17.2 mm. The fluence volume of both 8.2 mm and 29.2 mm lens distance is smaller.

4. Energy transfer

The transmitted energy from laser to plasma was determined by using a fast photodiode. Therefore, the temporal pulse profiles for different laser energies were measured with and without optical breakdown. The optical breakdown is characterized by a sharp falling edge within the temporal pulse profile. Measurements without optical breakdown were realized by replacing the focusing unit by an expanding lens to expand the laser beam. Plasma was induced by using different lens distances of expanding lens and focusing lens. The results are shown in Fig. 7(a) exemplarily for a 4.7 mJ laser pulse and seven different lens distances. It is evident that the optical breakdown occurs earlier for higher lens distances and thus, for higher maximum fluences. The area below the temporal pulse profiles corresponds to the transmitted energy which is not absorbed by the plasma. The transmitted energy decreases with increasing lens distances and consequently the absorbed energy increases. The difference of the area below the pulse profiles without and with breakdown is the amount of energy absorbed by the plasma. In Fig. 7(b), the amounts of absorbed energy for different laser energies and lens distances are summarized. Errors are determined by the law of error propagation and are indicated by error bars. The results were verified by measurements with a pyroelectric detector (PE50, Ophir, triangles). It can be seen that the energy transfer efficiency increases with higher laser energy [Fig. 7(b)]. Furthermore, it is indicated that the transferred energy increases with increasing lens distance which corresponds to higher maximum fluences. The amount ranges from 36% to 86% depending on pulse energy and lens distance.

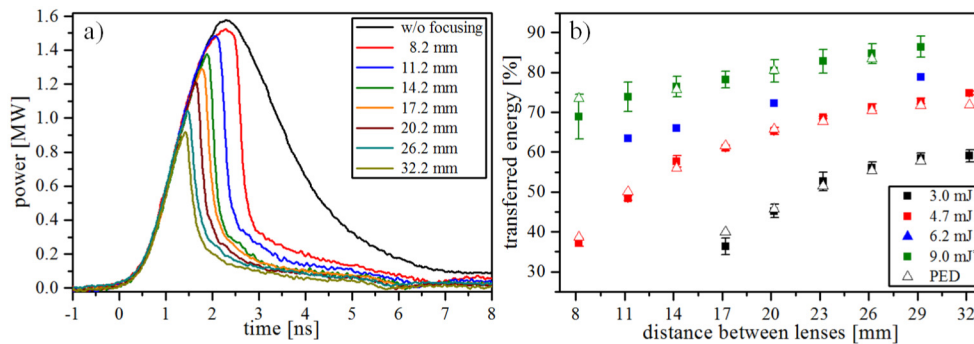


Fig. 7. (a) Temporal pulse profile of the 4.7 mJ laser pulse at different lens distances and without focusing. (b) Transferred energy at different lens distances for various laser energies. (* indicates different pulse properties)

Figure 7(b) demonstrates that the highest amount of deposited energy occurs at a pulse energy of 9.0 mJ*, although the maximum fluence is below the level of maximum fluence of 6.2 mJ pulses. This could be explained by the transmitted energies at different laser energies and lens distances [Fig. 8]. The transmitted energy is almost identical for each lens distance and independent of the laser energy. According to Brieschenk et al. [32], the transmitted energy is equal to the breakdown energy threshold and the breakdown energy threshold depends on laser properties, e. g. pulse intensity distribution, pulse length, beam intensity distribution, diameter etc. Consequently, breakdown energy thresholds of laser pulses with different pulse energies are identical, if laser beam properties and focusing parameters are similar.

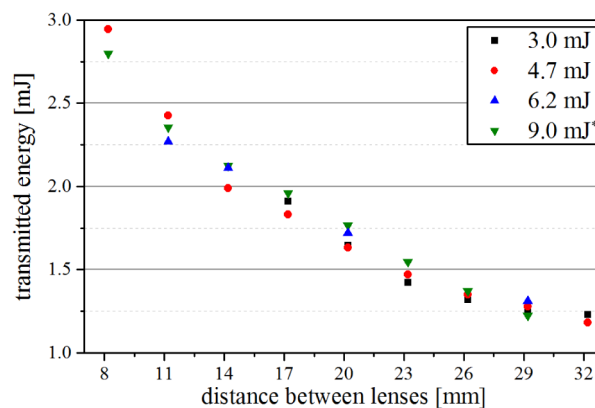


Fig. 8. Transmitted energy at different lens distances. (* indicates different pulse properties)

In the presented case, this means that the breakdown energy threshold is the same for all energy levels at a specific lens distance, thus, laser pulse properties of pulses with different energy should be comparable. This is the case for laser pulses up to 6.2 mJ pulse energy (Table 1). The beam width d_{laser} and the beam quality factor M^2 are significantly higher for the 9.0 mJ* laser pulse than for pulses with lower laser energies. Consequently, the breakdown energy threshold and, therefore, the transmitted energy should be different to lower pulse energies. To explain this, the 2D-beam intensity profiles from all analyzed laser pulses are considered again [Fig. 4]. It can be seen that the beam profile is almost radially symmetric at low energy levels up to 6.2 mJ. Just the 9.0 mJ* laser pulse shows strong bulges at the edge of the beam profiles. However, the center of the beam profiles can be assumed as radially symmetric, even for laser beams with 9.0 mJ* pulse energy. Lorenz et al. [21] have recently demonstrated that the outer areas of laser pulses from end pumped passively q-switched lasers

are emitted later in time than inner areas. Furthermore, the beam quality factor M^2 does not take the spatial-temporal emission profile of the laser pulse into consideration. In this case, it is supposed that the high beam quality factor is caused by the outer areas of the pulse profile, which are emitted at later times, more specifically after optical breakdown. Hence, beam properties of the laser pulses with different energy levels are assumed to be similar at the time of breakdown and breakdown energy threshold is approximately equal.

5. Plasma evolution and propagation

This chapter deals with the plasma evolution during and after the laser pulse. In the first section, plasma evolution during the laser pulse and the influence of different focusing configurations are discussed. Quantitative analysis of plasma propagation after the laser pulse are presented in the second section.

5.1 Plasma imaging during energy transfer

For generation of laser induced plasma via non-resonant breakdown, different processes are involved. In a first step, initial electrons have to be produced. Multiphoton ionization occurs only at short wavelengths or at very low pressure [33,34]. Raizer [35], Yablonoitch [36] and Kopececk et al. [12] attribute the generation of initial free electrons to impurities in the gas mixture, which absorb laser radiation. This results in high local temperatures. Plasma breakdown takes place in a very small region at the focal spot due to processes like photon absorption via inverse bremsstrahlung and cascade ionization [37,38]. The highly ionized layer absorbs the laser light and turns into an absorption layer [37], which propagates like a wave along the laser beam towards the beam direction until the end of laser emission [25,37]. The propagation of the absorption layer is also called laser supported detonation wave. The velocity of this absorption wave is about 100 km/s to 200 km/s depending mainly on the power density in the focal region [37,39]. After the end of the laser pulse, the plasma and, therefore, the absorption wave, is not supplied with energy anymore. The plasma cools down and expands evenly in all direction, until it is in equilibrium with the surrounding gas [40].

To investigate the temporal behavior of optical breakdown and spontaneous plasma emission in dependency of laser pulse emission, temporal profiles of laser pulse and plasma emission were measured with fast photodiodes. The profiles are displayed in Fig. 9. It can be seen that the plasma emission (blue line) starts shortly after the plasma breakdown indicated by the sharp falling edge in the laser pulse profile (red line). The intensity of the plasma emission increases strongly and reaches the maximum nearly at the end of the laser pulse (red dashed line). After irradiation of the laser pulse, the plasma cools down and the intensity of plasma emission declines within a view hundred nanoseconds.

To discuss plasma propagation after the breakdown and during the laser radiation, plasma images were taken with an intensified CCD camera (chapter 2.2). Images made during and after the laser pulse can be seen in Fig. 9 on the right side and on the left side, respectively. The numbers within the images are linked with the numbers in the diagram and indicate the moment of recording. The intensifier gain of the ICCD camera was kept constant for all plasma records. The exposure time was set to 2.88 ns for plasma records during and shortly after the laser pulse emission. Plasma images starting 32 ns (7-9) after the optical breakdown were recorded with an exposure time of 10 ns. The marked time in Figs. 9 and 10 corresponds to the end of the exposure time. The laser pulse has a pulse energy of 3 mJ and the lens distance was set to 29.2 mm. Images are normalized to the maximum intensity of each recording to reveal the plasma structure at each time delay. Two phases can be distinguished during the plasma evolution: a first phase of plasma evolution during laser pulse emission and a second phase after the laser pulse.

Shortly after breakdown (1) plasma has not developed a defined shape. After nearly one nanosecond, the plasma has the characteristic teardrop-like shape (2). Until the end of the laser pulse, the plasma propagates primarily towards the laser beam direction. Also, the position of maximum intensity shifts in the same direction. This is caused by the previously discussed laser supported radiation wave. According to the authors' knowledge this is the first

time a laser supported radiation wave is recorded after laser induced breakdown with a PQL. After the laser pulse (2nd phase), the plasma is not supplied with energy anymore. Thus, plasma expansion is accompanied by an intensity decay, as can be seen in Fig. 9. The plasma disappears the teardrop-like shape and intensity distribution within the plasma becomes more homogenous (6). During the decrease of intensity, the plasma expands in all directions. The decreasing intensity is accompanied by a decay of the plasma temperature [41]. The temperature decay is mainly caused by losses due to shock wave generation, radiation and bremsstrahlung [40]. A non-uniform plasma formation characterized by several hotspots within the plasma shape as observed by several groups [10,42–44] is not observed in this study. In literature, the non-uniform formation is referred to spherical aberrations of applied lenses [42,45,46]. In these studies, converging lenses with focal length of 50 mm to 300 mm are used. In contrast, in our experiments effective focal lengths of 6 mm to 15 mm result from using a concave and a convex lens for focusing. Furthermore, an aspheric focusing lens is used. It is assumed that this leads to a more uniform plasma formation.

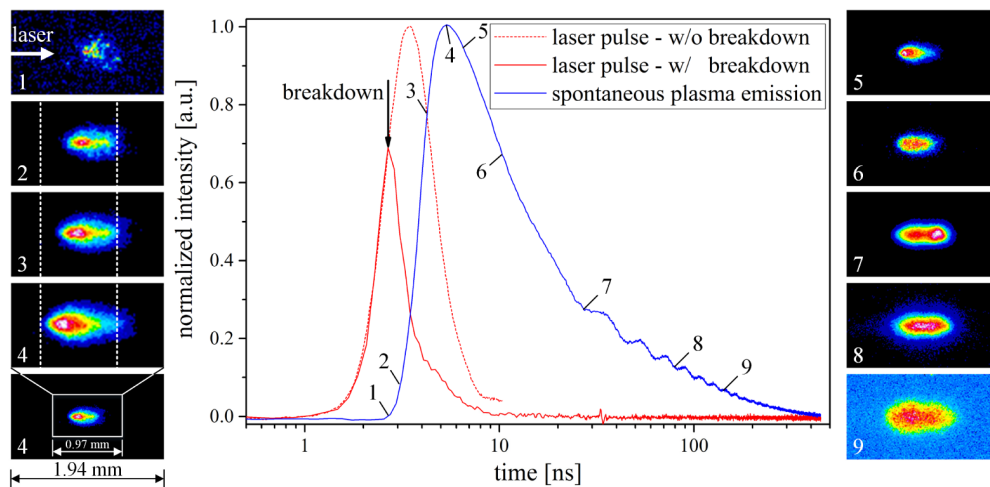


Fig. 9. Temporal laser pulse profile with and without focusing and temporal evolution of total intensity of plasma emission after breakdown (3 mJ, lens distance 29.2 mm).

As mentioned above, the plasma develops a teardrop-like shape in the first 4 to 5 ns of plasma emission, which corresponds to the time of plasma breakdown at the end of the laser pulse [Fig. 9, left side]. On the laser averted side, the plasma shows a conical shape with a characteristic angle for each distance of the concave and focusing lens. A series of images of the first five nanoseconds of plasma development for different lens distances is illustrated in Fig. 10. The plasma records are normalized to the maximum of each moment in time. It can be seen that the angle of the conical shape becomes larger with increasing lens distance. It was found that the angles at each lens distance correspond with the angle of the focused laser beam path. That means that the plasma follows the trace of the beam during laser emission. Furthermore, the dimension of the plasmas at different lens distances differ among each other. The length of the plasma decreases with higher lens distances and therefore larger focusing angles, whereas the height of the plasma increases. This may be explained by the beam paths at different lens distances. The angle of the focused beam increases with increasing lens distance. Thus, the beam waist is more tightened and the focal radius decreases, but the laser beam expands more rapidly towards laser direction. Because the plasma propagates along the beam path, the height of the plasma becomes bigger for higher focusing angles. In the case of smaller focusing angles, the laser beam path expands less towards the laser beam direction. Hence, the power density decreases more slowly along the beam path and the absorption wave propagates faster than for larger focusing angles. As a result, the plasma length becomes larger.

Furthermore, Fig. 10 demonstrates a rising intensity of plasma emission for larger lens distances (decreasing effective focal length). This can be attributed to an increased energy transfer due to higher maximum fluences in the case of larger lens distances.

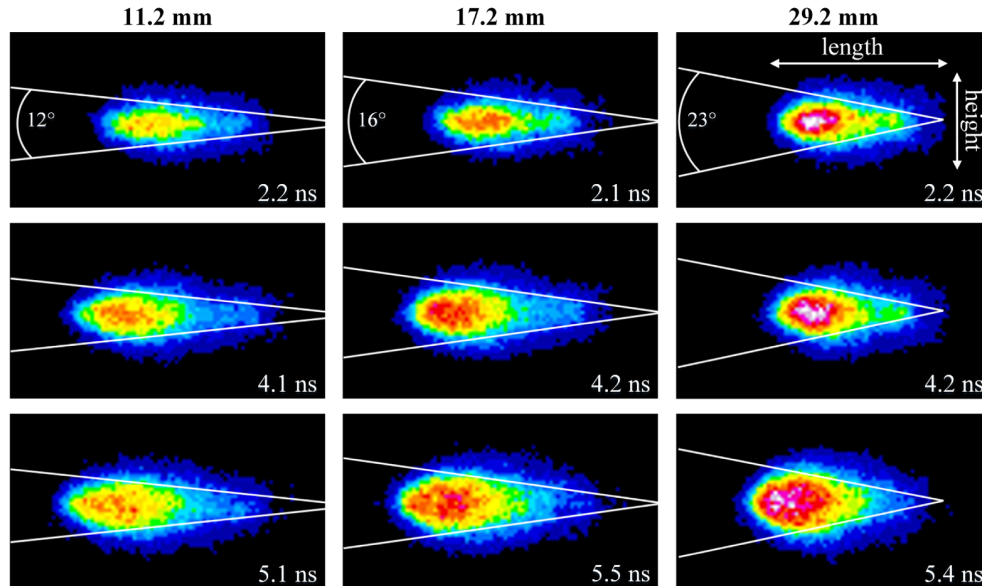


Fig. 10. Temporal series of plasma images at different lens distances (laser energy 6.2 mJ, dimension of images: 0.53 mm x 0.95 mm).

5.2 Plasma propagation after energy transfer

For the investigation of the influence of laser energy and focusing parameters on plasma expansion after laser irradiation, plasma images are performed for delay times up to 500 ns. The same experimental setup is used as for plasma imaging during energy transfer, but camera is triggered by the laser pulse itself. Therefore, the first image is recorded 50 ns after laser pulse. Camera settings like intensifier gain and exposure time (10 ns) are identical for all measurements. Plasma images are analyzed with respect to height, length and plasma volume. For analyzing these values, an intensity threshold is determined. The region exceeding this intensity threshold is associated to the geometry of the plasma. Intensity threshold is set to 10% of the maximum intensity of the plasma at each time delay. Similar threshold amounts were used by Glumac et al. [41]. For each time delay 50 independent breakdown events are recorded and calculations are averaged.

As mentioned above, plasma length and height behave contrarily. The length becomes smaller and the height larger for increasing lens distances respectively focusing angle. In Fig. 11, quantitative analysis of the temporal evolution of the plasma width and height are presented for a 9.0 mJ* laser pulse. Height and width increase for the first 150 ns to 200 ns and decrease afterwards. This temporal profile is qualitatively the same for all lens distances. For early time delays (up to 150 ns), plasma length is reduced by large lens distances. After reaching its maximum, the plasma length decreases more rapidly at lens distances of 8.2 mm and 11.2 mm. This is attributed to the little energy content due to a minor energy transfer from laser pulse to plasma. The influence of lens distances above 11.2 mm is not significant. Furthermore, the height enlarges by using larger lens distances. At high lens distances (17.2 mm – 29.2 mm), the height expansion is nearly equal. Quantitative analysis of plasma volume evolution is shown in Fig. 12. The plasma volume is evaluated by the assumption of a rotationally symmetric plasma. The evolution of the plasma volume behaves similarly to the height of the plasma.

A possible explanation for the behavior of the plasma evolution is the behavior of the fluence volume. Both, plasma volume and fluence volume increase for lens distances up to 14.2 mm [Figs. 12 and 6(b)]. By increasing the lens distance above 17.2 mm, the fluence volume is slightly reduced, but plasma volume stagnates. It is concluded that the decreasing fluence volume is compensated by the increasing maximum fluence and hence, the plasma volume remains nearly constant. This behavior of plasma evolution is qualitatively similar for the other laser energies of 3.0 mJ, 4.7 mJ and 6.2 mJ. There are only small differences at which lens distance the plasma expansion stagnates, due to differences in fluence volume characteristics for various laser energies. The influence of the laser energy on the plasma volume expansion is illustrated in Fig. 13. For clarity, results are only depicted for a representative lens distance of 26.2 mm. It is shown that the plasma volume increases for higher laser energies. Plasma expansion of a laser pulse of 4.7 mJ and 6.2 mJ is quite similar, only in the first 200 ns the plasma volume is larger in the case of a 6.2 mJ pulse.

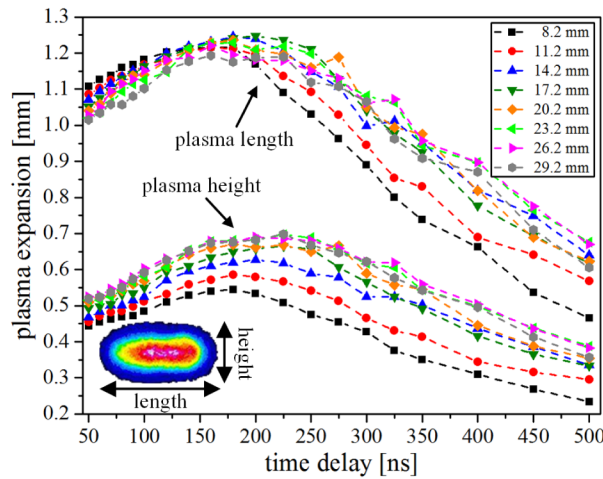


Fig. 11. Temporal expansion of length and height of plasma emission referred to a threshold of 10% of maximum intensity (laser pulse energy 9.0 mJ*).

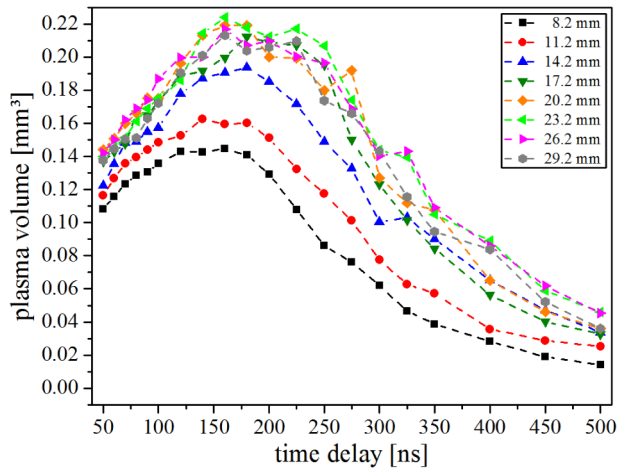


Fig. 12. Temporal expansion of plasma volume referred to a threshold of 10% of maximum intensity (laser pulse energy 9.0 mJ*).

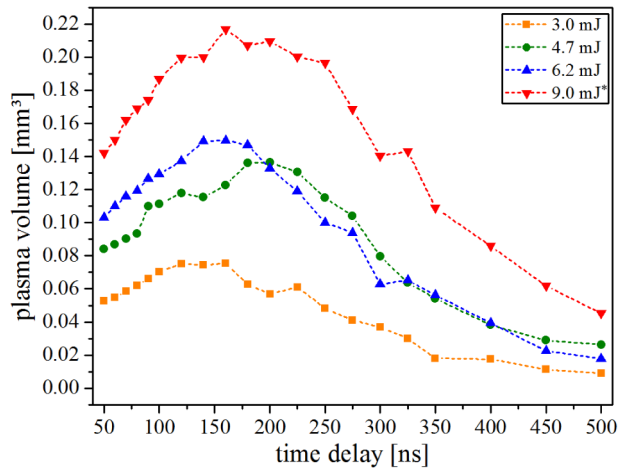


Fig. 13. Temporal evolution of plasma volume for different laser energies referred to a threshold of 10% of maximum intensity (distance between lenses 26.2 mm). (* indicates different pulse properties)

6. Conclusion

Optical breakdown was initiated with a PQL ignition system. Its focusing unit is built up from an expanding and a focusing lens, thus optical configuration can be varied by changing the lens spacing. Focal point properties are characterized by maximum fluence and fluence volume. Transferred energy is measured via the temporal pulse shape of the transmitted laser energy. In the case of similar laser pulse energies (3.0 mJ – 6.2 mJ) the results demonstrate that the transmitted laser energy only depends on the optical configuration, but not on the laser pulse energy. The amount of transferred energy is in the range of 36% and 79% depending on the pulse energy and the optical configuration. The transferred energy increases with increased pulse energy and lens spacing (decreasing effective focal length) and thus, with increased maximum fluence. The transmitted energy remains unchanged even in the case of different laser pulse properties (9 mJ laser pulse). As a consequence, transferred energy is on a higher level than for laser pulses with lower laser energies, although maximum fluence is reduced.

Plasma evolution during the energy transfer from laser to plasma and after the laser pulse is investigated temporally and spatially highly resolved. During laser pulse emission, the plasma follows the beam path towards the laser direction due to a laser supported detonation wave. A characteristic angle of the conical shape of the plasma can be found. The angle corresponds to the angle of the focused laser beam. After the laser pulse, the plasma is not supplied with energy anymore and plasma propagates the same in all directions. A rising fluence volume results in an increased plasma volume, but expansion saturates when the fluence volume reaches its maximum.

Acknowledgments

The authors are grateful for the financial support of the German Research Foundation (DFG) under grant no. BR 1713/13-1. Furthermore, the authors thank the Robert Bosch GmbH for the numerous helpful discussions and the laser ignition system granted as a loan. The authors also thank Ophir photonics for providing the beam propagation analyzer M²-200s-FW. This publication was funded by the German Research Foundation (DFG) and the University of Bayreuth in the funding programme Open Access Publishing